

RESEARCH ARTICLE

Detection and prebiotic chemistry of possible glycine precursor molecule methylenimine towards the hot molecular core G10.47+0.03

Arijit Manna  and Sabyasachi Pal 

Department of Physics and Astronomy, Midnapore City College, Paschim Medinipur, 721129 India

Corresponding author: Sabyasachi Pal; Email: sabya.pal@gmail.com

Received: 22 July 2023; **Revised:** 1 March 2024; **Accepted:** 21 March 2024

Keywords: Astrochemistry, interstellar medium, millimetre astronomy, prebiotic chemistry, star-formation region

Abstract

Amino acids are essential for the synthesis of protein. Amino acids contain both amine ($R-NH_2$) and carboxylic acid ($R-COOH$) functional groups, which help to understand the possible formation mechanism of life in the universe. Among the 20 types of amino acids, glycine (NH_2CH_2COOH) is known as the simplest non-essential amino acid. In the last 40 years, all surveys of NH_2CH_2COOH in the interstellar medium, especially in the star-formation regions, have failed at the millimetre and sub-millimetre wavelengths. We aimed to identify the possible precursors of NH_2CH_2COOH , because it is highly challenging to identify NH_2CH_2COOH in the interstellar medium. Many laboratory experiments have suggested that methylenimine (CH_2NH) plays a key role as a possible precursor of NH_2CH_2COOH in the star-formation regions via the Strecker synthesis reaction. After spectral analysis using the local thermodynamic equilibrium (LTE) model, we successfully identified the rotational emission lines of CH_2NH towards the hot molecular core G10.47+0.03 using the Atacama Compact Array (ACA). The estimated column density of CH_2NH towards G10.47+0.03 is $(3.40 \pm 0.2) \times 10^{15} \text{ cm}^{-2}$ with a rotational temperature of $218.70 \pm 20 \text{ K}$, which is estimated from the rotational diagram. The fractional abundance of CH_2NH with respect to H_2 towards G10.47+0.03 is 2.61×10^{-8} . We found that the derived abundance of CH_2NH agree fairly well with the existing two-phase warm-up chemical modelling abundance value of CH_2NH . We discuss the possible formation pathways of CH_2NH within the context of hot molecular cores, and we find that CH_2NH is likely mainly formed via neutral–neutral gas-phase reactions of CH_3 and NH radicals towards G10.47+0.03.

Contents

Introduction	1
Observation and data reductions	4
Result	4
Continuum emission towards the G10.47+0.03	4
Identification of the CH_2NH in the G10.47+0.03	5
Rotational diagram analysis of CH_2NH	6
Spatial distribution of CH_2NH in the G10.47+0.03	7
Discussion	9
CH_2NH towards the G10.47+0.03	9
Comparison with modelled and observed abundance of CH_2NH	10
Searching of NH_2CH_2COOH towards the G10.47+0.03 using the ACA	10
Conclusion	11

Introduction

At millimetre and submillimetre wavelengths, approximately 290 prebiotic and complex organic molecules have been discovered in the interstellar medium (ISM) or circumstellar shells¹. The identification of complex prebiotic molecules in the ISM is important to understand the chemical evolution of biologically relevant prebiotic molecules from fundamental molecular species (Herbst and van Dishoeck, 2009). Hot molecular cores are one of the early stages of high-mass star-formation regions (van Dishoeck and Blake, 1998; Herbst and van Dishoeck, 2009; Shimonishi *et al.*, 2021; Manna *et al.*, 2023; Manna and Pal, 2024a). The early stages of the high-mass star-formation regions are known as the chemically rich phase, which plays an essential role in understanding the formation of chemical complexity in the ISM (Tan *et al.*, 2014; Shimonishi *et al.*, 2021). In the hot molecular cores, the complex organic molecules escape from the icy surfaces of dust grains, or the complex organic molecules are created in the hot circumstellar gas (Herbst and van Dishoeck, 2009). Hot molecular cores are identified by their high gas density ($>10^6$ cm⁻³), small source size (<0.1 pc) and warm temperature (>100 K) (van Dishoeck and Blake, 1998; Kurtz *et al.*, 2000). The warm-up time scale for hot molecular cores ranges from $\sim 10^4$ to $\sim 10^6$ years (van Dishoeck and Blake, 1998; Garrod and Herbst, 2006; Garrod, 2013). The hot molecular phase is characterized by the rich molecular spectra of several complex organic molecules such as methanol (CH₃OH) and methyl cyanide (CH₃CN) (Allen *et al.*, 2017). These complex molecules can form on the surface of dust grains on a cooler surface and are then released when the grains are heated owing to the formation of stars (Allen *et al.*, 2017; Manna *et al.*, 2023). Alternatively, these complex molecules may be created in massive young objects when the high temperature (>100 K) allows for endothermic reactions (Allen *et al.*, 2017). Therefore, both formation pathways of complex organic molecules are important for acquiring molecular abundance around the hot molecular cores. Higher spectral and spatial resolution observations are required to identify the different complex organic molecules and the spatial distribution of these molecules in hot molecular cores. The detection of disc candidates in hot molecular cores is extremely rare, implying a link between the hot molecular core chemistry and discs (Allen *et al.*, 2017). Studying the chemistry of the hot molecular cores of disc candidates can help us to understand the chemical evolution of high-mass star formations on small physical scales (Allen *et al.*, 2017).

The disc-like hot molecular core G10.47+0.03 is known as the ultra-compact (UC) H II region, which is located at a distance of 8.6 kpc with a luminosity of $5 \times 10^5 L_{\odot}$ (Cesaroni *et al.*, 2010; Sanna *et al.*, 2014). G10.47+0.03 is a disc-like candidate because, in this source, the hot core is embedded in the disc (Sanna *et al.*, 2014; Manna and Pal, 2022a). Earlier, Rolffs *et al.* (2011) conducted a molecular spectral line survey of G10.47+0.03, using the Submillimeter Array (SMA) telescope in the frequency range of 199.9–692.2 GHz. Using the local thermodynamic equilibrium (LTE) modelling, Rolffs *et al.* (2011) detected the rotational emission lines of several simple and complex organic molecules such as sulphur monoxide (SO), sulphur dioxide (SO₂), cyanide (CN), hydrogen cyanide (HCN), hydrogen isocyanide (HNC), formamide (NH₂CHO), cyanoacetylene (HC₃N), vinyl cyanide (C₂H₃CN), formaldehyde (H₂CO), ethynol (H₂C₂O), ethanol (C₂H₅OH), dimethyl ether (CH₃OCH₃), methyl formate (CH₃OCHO), methanol (CH₃OH) and acetone (CH₃COCH₃) towards the G10.47+0.03. The rotational emission lines of methylamine (CH₃NH₂) and amino acetonitrile (NH₂CH₂CN) are also detected towards the G10.47+0.03 (Ohishi *et al.*, 2019; Manna and Pal, 2022a). The CH₃NH₂ and NH₂CH₂CN molecules are known to be other possible precursors of the simplest amino acid, NH₂CH₂COOH, towards hot molecular cores. The emission lines of cyanamide (NH₂CN) and ethyl cyanide (C₂H₅CN) are detected from the hot molecular core G10.47+0.03 using ALMA (Manna and Pal, 2022b, 2023a). Recently, the rotational emission line of phosphorus nitride (PN) is detected towards the G10.47+0.03 (Manna and Pal, 2024b).

The asymmetric top-molecule methylenimine (CH₂NH) is known to be a possible precursor of NH₂CH₂COOH in the ISM. The CH₂NH molecule was created by the hydrogenation of HCN on

¹<https://cdms.astro.uni-koeln.de/classic/molecules>

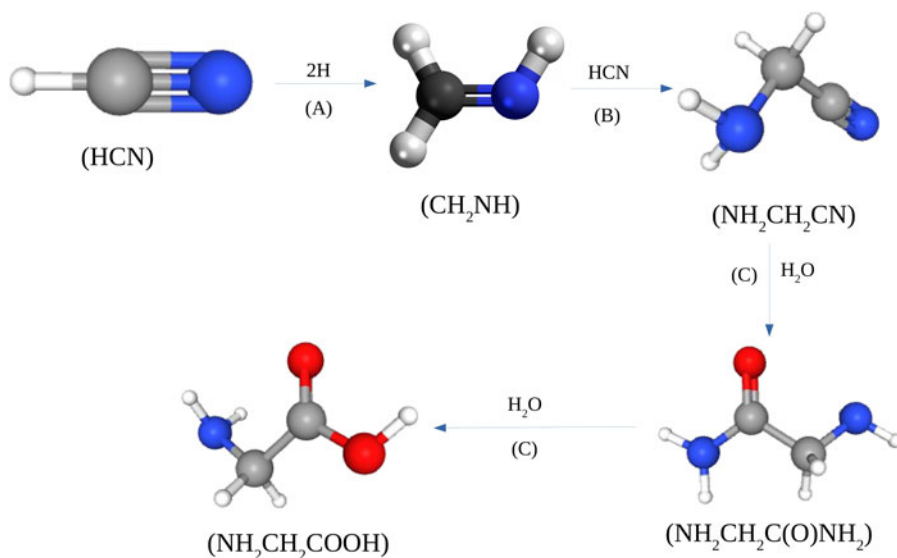


Figure 1. Proposed possible formation mechanism of CH_2NH and $\text{NH}_2\text{CH}_2\text{COOH}$. In the chemical diagram, the black/grey dumbbells indicate the carbon (C) atom, the white dumbbells indicate the hydrogen (H) atom, the blue dumbbells indicate the nitrogen (N) atom and the red dumbbells indicate the oxygen (O) atom. In the chemical reaction, ‘ H_2O ’ represents the hydrolysis process. References: (A) Woon (2002); Theule et al. (2011); (B) Danger (2011); (C) Alonso et al. (2018).

the dust surface of hot molecular cores (Woon, 2002; Theule *et al.*, 2011). When CH_2NH and HCN both react with each other via the Strecker synthesis reaction, the complex amino and nitrile-bearing molecule amino acetonitrile ($\text{NH}_2\text{CH}_2\text{CN}$) is produced (Danger, 2011). The hydrolysis of $\text{NH}_2\text{CH}_2\text{CN}$ on the grain surface creates glycnamide ($\text{O}(\text{NH}_2)$) (Alonso *et al.*, 2018). Finally, $\text{NH}_2\text{CH}_2\text{COOH}$ can be created via hydrolysis of $\text{NH}_2\text{CH}_2\text{C}(\text{O})\text{NH}_2$ on the grain surface of hot molecular cores (Alonso *et al.*, 2018). The proposed formation processes for CH_2NH and $\text{NH}_2\text{CH}_2\text{COOH}$ are shown in Fig. 1. Earlier, Suzuki *et al.* (2016) claimed that the CH_2NH molecule is created in the gas phase between the reactions of CH_3 and NH ($\text{CH}_3 + \text{NH} \rightarrow \text{CH}_2\text{NH}$). Quantum chemical studies have shown that CH_3NH_2 is produced via the sequential hydrogenation of CH_2NH (Joshi and Lee, 2022). This indicates that both CH_2NH and CH_3NH_2 are chemically linked in ISM (Joshi and Lee, 2022). Subsequently, Garrod *et al.* (2022) confirmed that both CH_2NH and CH_3NH_2 are chemically linked towards hot molecular cores by using three-phase warm-up chemical models. Both Joshi and Lee (2022) and Garrod *et al.* (2022) showed that CH_3NH_2 and CH_2NH are chemically connected with $\text{NH}_2\text{CH}_2\text{COOH}$. Previously, many authors claimed that CH_2NH was detected in the high-mass star-formation region Sgr B2. Evidence of CH_2NH was found near Sgr B2 (OH) (Godfrey *et al.*, 1973; Turner, 1989), Sgr B2 (N) (Halfen *et al.*, 2013) and Sgr B2 (M) (Sutton *et al.*, 1991). Previously, Jones *et al.* (2008, 2011) created the spatial distribution of CH_2NH from Sgr B2 (N) to Sgr B2 (S) at wavelengths of 3 and 7 mm using the MOPRA telescope. Belloche *et al.* (2013) demonstrated a detailed analysis of CH_2NH towards the Sgr B2 (N) and Sgr B2 (M) using the IRAM 30 m telescope. The rotational emission lines of CH_2NH were also detected for W51 e1/e2, Orion KL, G34.3+0.15, G19.61-0.23, IRAS 16293–2422 B and NGC 6334I (Dickens *et al.*, 1997; White *et al.*, 2003; Qin *et al.*, 2010; Ligterink *et al.*, 2018; Bøgelund *et al.*, 2019). Recently, CH_2NH megamaser² lines were detected in six compact obscured nuclei using the Very Large Array (VLA) (Gorski *et al.*, 2021).

²A megamaser is a type of astrophysical maser in which the luminosities of the spectral lines are 100 million times brighter than normal masers emission lines in the ISM.

In this article, we present the identification of the possible $\text{NH}_2\text{CH}_2\text{COOH}$ precursor molecule CH_2NH towards the G10.47+0.03, using ACA. To estimate the column density and rotational temperature of CH_2NH , we used a rotational diagram model. ACA observations and data reductions are presented in section ‘Observation and data reductions’. The results of the detection of the emission lines of CH_2NH are presented in section ‘Result’. The discussion and conclusion of the detection of CH_2NH are presented in sections ‘Discussion’ and ‘Conclusion’.

Observation and data reductions

We used the archival data of G10.47+0.03 in cycle 4, which was observed using the Atacama Compact Array (ACA) with a 7 m array (PI: Rivilla, Victor; ID: 2016.2.00005.S). The ACA is the heart of the Atacama Large Millimeter/submillimeter Array (ALMA). The observed phase centre of the hot molecular core G10.47+0.03 is $(\alpha, \delta)_{\text{J2000}} = 18 : 08 : 38.232, -19:51:50.400$. The observation was carried out on 16 September 2017, using 11 antennas. The observations were made with ACA band 4 with spectral ranges of 127.47–128.47, 129.74–130.74, 139.07–140.07 and 140.44–141.44 GHz and a corresponding spectral resolution of 488 kHz. During the observation, the flux calibrator and bandpass calibrator were J1924–2914, and the phase calibrator was J1833–210B.

For data reduction and imaging, we used the Common Astronomy Software Application (CASA 5.4.1) with an ALMA data reduction pipeline (McMullin *et al.*, 2007). The data analysis flow chart is shown in Manna and Pal (2024). For flux calibration using the flux calibrator, we used the Perley-Butler 2017 flux calibrator model for each baseline to scale the continuum flux density of the flux calibrator using the CASA task SETJY (Perley and Butler, 2017). We constructed the flux and bandpass calibration after flagging bad antenna data and channels using the CASA pipeline with tasks `hifa_bandpassflag` and `hifa_flagdata`. After the initial data reduction, we used the task MSTRANSFORM with all available rest frequencies to separate the target data of G10.47+0.03. For continuum and background subtraction, we used task UVCONTSUB in the UV plane of the separated calibrated data. We used the CASA task TCLEAN with a Briggs weighting robust value of 0.5, to create continuum and spectral images of the G10.47+0.03. To produce spectral images, we used the SPECMODE = CUBE parameter in the TCLEAN task. The final spatial resolutions of the spectral data cubes were $10.48'' \times 6.28''$, $10.82'' \times 6.39''$, $12.08'' \times 6.90''$ and $12.08'' \times 6.79''$ between the frequency ranges of 127.47–128.47, 129.74–130.74, 139.07–140.07 and 140.44–141.44 GHz with a spectral resolution of 488.28 kHz. Finally, we used the CASA task IMPBCOR to correct the primary beam pattern in continuum images and spectral data cubes.

Result

Continuum emission towards the G10.47+0.03

We presented the continuum emission images of the hot molecular core G10.47+0.03 at frequencies of 127.97, 130.25, 139.56 and 140.92 GHz. The continuum images are shown in Fig. 2, where the surface brightness colour scale has units of the Jy beam^{-1} . After the creation of the continuum emission images, we fitted the 2D Gaussian over the continuum emission images using the CASA task IMFIT and estimated the integrated flux density in Jy, peak flux density in Jy beam^{-1} , synthesized beam size in arcsec ($''$), deconvolved beam size in arcsec ($''$), position angle in degrees ($^\circ$) and RMS in mJy of the hot core G10.47+0.03. The estimated continuum image properties of hot core G10.47+0.03 are shown in Table 1. We noticed that the continuum emission region of G10.47+0.03 is smaller than the synthesized beam size, which was estimated after fitting the 2D Gaussian over the continuum emission region. This indicates that the continuum emission image of G10.47+0.03 was not resolved between the frequency range of 127.97 and 140.92 GHz. Recently, Manna and Pal (2023a) reported the detection of continuum emission from the G10.47+0.03 in the frequency range of 130.23–160.15 GHz with a flux density variation of 1.36–2.71 Jy.

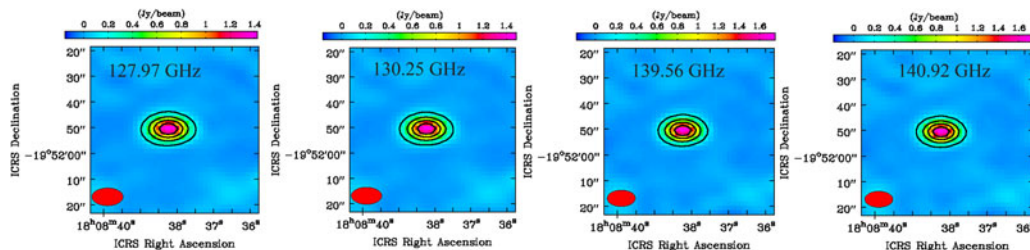


Figure 2. Millimetre-wavelength continuum emission images of the hot molecular core G10.47+0.03. Continuum emission images are obtained with ACA band 4 at frequencies of 127.97, 130.25, 139.56 and 140.92 GHz. The contour levels start at 3σ , where σ is the RMS of each continuum image. The contour levels increase by a factor of $\sqrt{2}$. The red circles indicate the synthesized beams of the continuum images. The corresponding synthesized beam sizes and RMS values of all continuum images are presented in Table 1.

Table 1. Summary of the millimetre wavelength continuum images of G10.47+0.03

Frequency (GHz)	Wavelength (mm)	Integrated flux (Jy)	Peak flux (Jy beam ⁻¹)	Beam size (″×″)	Deconvolved source size (″×″)	RMS (mJy)	Position angle (°)
127.97	2.34	1.57±0.01	1.44±0.08	12.02×6.87	2.60×2.18	9.16	-89.71
130.25	2.30	1.66±0.01	1.51±0.08	11.96×6.73	2.73×2.52	8.76	-89.63
139.56	2.14	1.98±0.02	1.78±0.01	10.73×6.35	2.71×2.29	10.72	-89.61
140.92	2.12	2.00±0.02	1.78±0.01	10.61×6.25	2.75×2.44	11.68	-89.91

Identification of the CH₂NH in the G10.47+0.03

First, we extracted the millimetre-wavelength molecular spectra from the spectral data cubes to create a 23.75″ diameter circular region over the G10.47+0.03. The synthesized beam sizes of the spectral data cubes of hot core G10.47+0.03 are 10.48″×6.28″, 10.82″×6.39″, 12.08″×6.90″ and 12.08″×6.79″. Hot core G10.47+0.03 is located at a distance of 8.6 kpc and at that distance, a $\sim 10''$ resolution refers to a spatial scale of 0.4 pc. This implies that the extracted spectrum mostly represents the outer envelope. The systematic velocity (V_{LSR}) of G10.47+0.03 is 68.50 km s⁻¹ (Rolffs *et al.*, 2011). We used the second-order polynomial to subtract the baseline of the entire spectra. To identify the rotational emission lines of CH₂NH, we used the LTE model with the Cologne Database for Molecular Spectroscopy (CDMS) database (Müller *et al.*, 2005). For LTE modelling, we used CASSIS (Vastel *et al.*, 2015). The LTE assumptions are valid in the inner region of G10.47+0.03 because the gas density of the warm inner region of the hot core is 7×10^7 cm⁻³ (Rolffs *et al.*, 2011). To fit the LTE model spectra of CH₂NH over the millimetre wavelength spectra of G10.47+0.03, we applied the Markov Chain Monte Carlo (MCMC) algorithm in CASSIS. After the LTE analysis, we have detected a total of three transitions of CH₂NH, i.e. $J=2(0, 2) - 1(0, 1)$, $J=6(2, 4) - 7(1, 7)$ and $J=10(3, 7) - 11(2, 10)$. The three detected transitions of CH₂NH had hyperfine lines. We do not discuss the hyperfine lines regarding the identified transitions of CH₂NH because the current spectral resolution is insufficient to resolve the hyperfine lines. The CH₂NH is a simple asymmetric top with all atoms being on the simple plane, and the transitions are described using labels of J' , K'_p , K'_o , and J'' , K''_p , K''_o . In the transition of CH₂NH, J indicated the total rotational angular momentum quantum number, K_p indicated the projection of J on the symmetry axis in the limiting prolate symmetric top, K_o indicated the projection of J on the symmetry axis in the limiting oblate symmetric top and F indicated the total

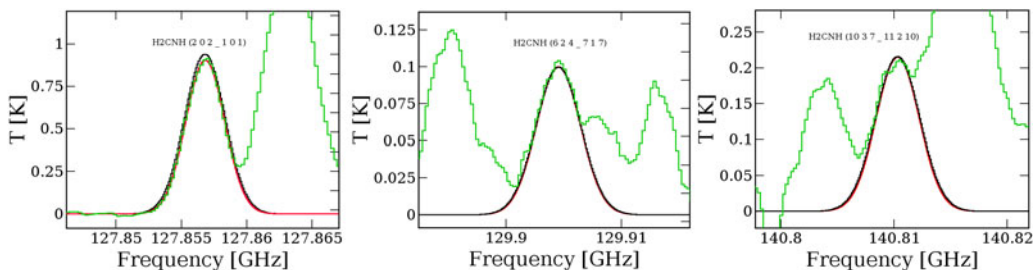


Figure 3. Identified rotational emission lines of CH_2NH towards the $G10.47+0.03$ in the frequency ranges of 127.47–128.47, 129.74–130.74 and 140.44–141.44 GHz. The green spectra indicate the millimetre-wavelength molecular spectra of $G10.47+0.03$. The black spectra present the best-fit LTE model spectra of CH_2NH , and the red spectra indicate the Gaussian model. The radial velocity of the spectra is 68.50 km s^{-1} .

Table 2. Summary of the molecular line parameters of the CH_2NH towards the $G10.47+0.03$

Frequency (GHz)	Transition ^a $J'(K'_p, K'_o) - J''(K''_p, K''_o)$	E_u^b (K)	A_{ij}^b (s^{-1})	g_{up}^b	$S\mu^{2c}$ (Debye ²)	FWHM ^d (km s^{-1})	$\int T_{\text{mb}} dV^d$ (K km s^{-1})	Optical depth (τ)
127.856	2(0,2)–1(0,1)	9.21	1.75×10^{-5}	15	10.76	9.49 ± 0.10	5.97 ± 0.25	2.96×10^{-4}
129.904	6(2,4)–7(1,7)	96.38	3.23×10^{-6}	39	4.93	9.62 ± 0.48	0.61 ± 0.06	4.87×10^{-4}
140.810	10(3,7)–11(2,10)	240.27	4.85×10^{-6}	63	9.41	9.56 ± 0.98	0.23 ± 0.09	8.51×10^{-4}

^aAll detected transitions of CH_2NH are also verified from Table 2 in Kirchoff *et al.* (1973) and CDMS molecular database.

^bThe values of E_{up} , A_{ij} and g_{up} are taken from the CDMS database.

^cThe line intensity $S\mu^2$ is defined by the product of the transition line strength S and square of the dipole moment μ^2 of CH_2NH . The values of $S\mu^2$ of detected transitions of CH_2NH are taken from online molecular database splatalogue.

^dFWHM and $\int T_{\text{mb}} dV$ are estimated from the fitting of the Gaussian model over the observed spectra of CH_2NH .

angular momentum quantum number, which includes the nuclear spin for the nucleus with the largest χ or eQq where χ or eQq denoted the nuclear electric quadrupole coupling constant along the indicated principal axis (Kirchoff *et al.*, 1973). There were no missing transitions of CH_2NH in the observable frequency ranges. As per the CDMS and online molecular database Splatalogue, we find that all the detected transitions of CH_2NH are not blended with other nearby molecular transitions. Using the LTE model, the best-fit column density of CH_2NH is $(3.21 \pm 1.5) \times 10^{15} \text{ cm}^{-2}$ with an excitation temperature of $210.50 \pm 32.82 \text{ K}$ and a source size of $10.78''$. The full-width half maximum (FWHM) of the LTE-fitted rotational emission spectra of CH_2NH is 9.5 km s^{-1} . The LTE-fitted rotational emission spectra of CH_2NH are shown in Fig. 3. After identifying the rotational emission lines of CH_2NH using the LTE model, we obtained the molecular transitions, upper-state energy (E_u) in K, Einstein coefficients (A_{ij}) in s^{-1} , line intensity ($S\mu^2$) in Debye² and optical depth (τ). We also verified the detected transitions of CH_2NH from Kirchoff *et al.* (1973). To estimate the proper FWHM and integrated intensity ($\int T_{\text{mb}} dV$) of the detected emission lines of CH_2NH , we fitted a Gaussian model to the observed spectra of CH_2NH . A summary of the detected transitions and spectral line properties of CH_2NH are presented in Table 2.

Rotational diagram analysis of CH_2NH

In this work, we used the rotational diagram method to estimate the total column density (N) in cm^{-2} and the rotational temperature (T_{rot}) in K of CH_2NH because we detected multiple transition lines of CH_2NH towards the $G10.47+0.03$. Initially, we assumed that the detected CH_2NH emission lines

were optically thin and populated under the LTE conditions. The equation of column density for optically thin molecular emission lines can be expressed as (Goldsmith and Langer, 1999),

$$N_u^{thin} = \frac{3g_u k_B \int T_{mb} dV}{8\pi^3 \nu S \mu^2} \quad (1)$$

where g_u is the degeneracy of the upper state, μ is the electric dipole moment, S indicates the strength of the transition lines, ν is the rest frequency, k_B is Boltzmann's constant and $\int T_{mb} dV$ indicates the integrated intensity. The total column density of CH₂NH under LTE conditions can be written as,

$$\frac{N_u^{thin}}{g_u} = \frac{N_{total}}{Q(T_{rot})} \exp(-E_u/k_B T_{rot}) \quad (2)$$

where E_u is the upper-state energy of CH₂NH, T_{rot} is the rotational temperature of CH₂NH and $Q(T_{rot})$ is the partition function at the extracted rotational temperature. The rotational partition function of CH₂NH at 75 K is 740.457, that at 150 K is 2084.970, and that at 300 K is 5892.504 (Müller *et al.*, 2005). Equation (2) can be rearranged as,

$$\ln\left(\frac{N_u^{thin}}{g_u}\right) = \ln(N) - \ln(Q) - \left(\frac{E_u}{k_B T_{rot}}\right) \quad (3)$$

Equation (3) indicates a linear relationship between the upper state energy (E_u) and $\ln(N_u/g_u)$ of CH₂NH. The value $\ln(N_u/g_u)$ was estimated using Equation (1). Equation (3) indicates that the spectral parameters with respect to the different transition lines of CH₂NH should be fitted with a straight line, whose slope is inversely proportional to the rotational temperature (T_{rot}), with its intercept yielding $\ln(N/Q)$, which will help estimate the molecular column density of CH₂NH. For the rotational diagram analysis, we estimated the spectral line parameters of CH₂NH after fitting the Gaussian model over the observed spectra of CH₂NH using the Levenberg–Marquardt algorithm in CASSIS (see section ‘Identification of the CH₂NH in the G10.47+0.03’ for details on spectral fitting). For the rotational diagram analysis, we used all the detected transitions of CH₂NH to estimate the accurate column density and rotational temperature because all the detected transitions of CH₂NH are non-blended. The resultant rotational diagram of CH₂NH is shown in Fig. 4, which was created using the ROTATIONAL DIAGRAM module in CASSIS. In the rotational diagram, the vertical red error bars indicate the absolute uncertainty of $\ln(N_u/g_u)$, which was determined from the estimated error of $\int T_{mb} dV$. From the rotational diagram, we estimated the column density of CH₂NH to be $(3.40 \pm 0.2) \times 10^{15} \text{ cm}^{-2}$ with a rotational temperature of $218.70 \pm 20 \text{ K}$. From the LTE spectral modelling, we found that the column density and excitation temperature of CH₂NH are $(3.21 \pm 1.5) \times 10^{15} \text{ cm}^{-2}$ and $210.50 \pm 32.82 \text{ K}$, which are nearly similar to the estimated column density and rotational temperature of CH₂NH using the rotational diagram model. Our derived rotational temperature of CH₂NH indicates that the detected transitions of CH₂NH arise from the warm-inner region of G10.47+0.03 because the temperature of the hot molecular core is above $\geq 100 \text{ K}$ (van Dishoeck and Blake, 1998). To determine the fractional abundance of CH₂NH, we use the column density of CH₂NH inside the 12.08'' beam and divide it by the column density of H₂. The estimated fractional abundance of CH₂NH towards G10.47+0.03 with respect to H₂ is 2.61×10^{-8} , where the column density of H₂ towards the G10.47+0.03 is $1.30 \times 10^{23} \text{ cm}^{-2}$ (Suzuki *et al.*, 2016).

Spatial distribution of CH₂NH in the G10.47+0.03

We created integrated emission maps of CH₂NH towards the G10.47+0.03, using the CASA task IMMOMENTS. Integrated emission maps of CH₂NH were created by integrating the spectral data cubes in the velocity ranges of 61.06–74.11, 63.80–75.28 and 64.40–70.93 km s⁻¹, where the emission lines of CH₂NH were detected. We created integrated emission maps for the three non-blended

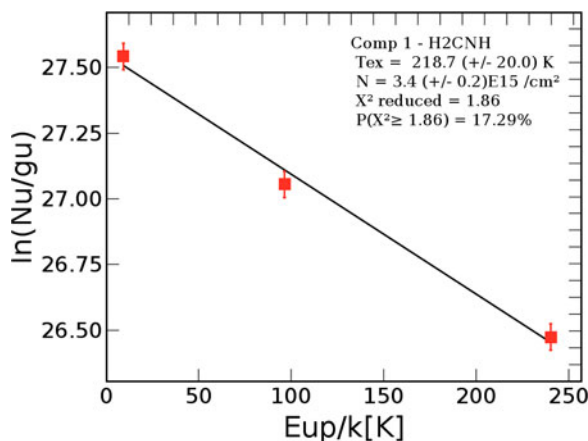


Figure 4. Rotational diagram of CH_2NH towards $G10.47+0.03$. In the rotational diagram, the red blocks represent the statistical data points of all detected transitions, and the solid black line indicates the fitted straight line, which helps estimate the column density and rotational temperature of CH_2NH .

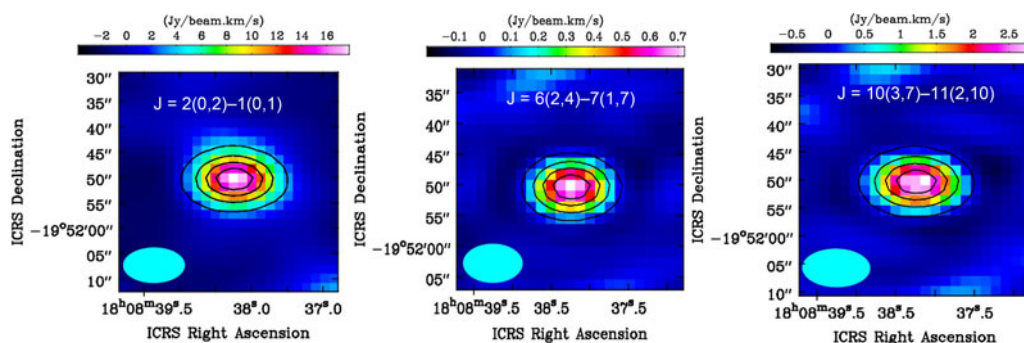


Figure 5. Integrated emission maps of detected transitions of CH_2NH towards the $G10.47+0.03$, which are overlaid with the 2.34 mm continuum emission map. The contour levels are at 20, 40, 60 and 80% of peak flux. The cyan circle represents the synthesized beam of the integrated emission maps.

transitions of CH_2NH towards the $G10.47+0.03$. The integrated emission maps of CH_2NH with different transitions towards the $G10.47+0.03$ are shown in Fig. 5. The resultant integrated emission maps of CH_2NH were overlaid with the 2.34 mm continuum emission map of $G10.47+0.03$. The integrated emission maps of CH_2NH exhibit a peak at the continuum position. From the integrated emission maps, it is evident that the transitions of the CH_2NH molecule arise from the warm inner part of the hot core region of $G10.47+0.03$. This indicates that the temperature of the detected transition lines of CH_2NH is above 100 K because the temperature of the hot core ≥ 100 K (van Dishoeck and Blake, 1998). From the rotational diagram, we estimate the temperature of CH_2NH is 218.7 ± 20 K, which indicates the emission lines of CH_2NH arise from the warm-inner region of $G10.47+0.03$. After the generation of the integrated emission maps of all identified lines of CH_2NH , we estimated the emitting regions of CH_2NH towards the $G10.47+0.03$ by fitting the 2D Gaussian over the integrated emission maps of CH_2NH using the CASA task IMFIT. The deconvolved beam size of the emitting region of CH_2NH was estimated by the following equation,

$$\theta_S = \sqrt{\theta_{50}^2 - \theta_{beam}^2} \quad (4)$$

where $\theta_{50} = 2\sqrt{A/\pi}$ indicates the diameter of the circle whose area (A) corresponds to the 50% line peak of CH_2NH and θ_{beam} is the half-power width of the synthesized beam (Rivilla *et al.*, 2017; Manna and Pal, 2022c, 2023b). The estimated emitting regions of the $J=2(0, 2) - 1(0, 1)$, $J=6(2, 4) - 7(1, 7)$, and $J=10(3, 7) - 11(2, 10)$ transitions of CH_2NH were $10.520''$ (0.44 pc), $10.275''$ (0.430 pc), and $10.781''$ (0.451 pc). The emitting region of CH_2NH varied between $10.520''$ and $10.781''$. We observed that the emitting regions of CH_2NH were similar or small with respect to the synthesized beam size of the integrated emission maps, which means that the transition lines of CH_2NH were not spatially resolved or, at best, marginally resolved. Therefore, we cannot draw any conclusions about the morphology of the integrated emission maps of CH_2NH towards the G10.47+0.03. Higher spectral resolution observations were needed using the ALMA 12 m array to solve the spatial distribution morphology of CH_2NH towards the hot molecular core G10.47+0.03.

Discussion

CH₂NH towards the G10.47+0.03

We presented the first interferometric detection of possible $\text{NH}_2\text{CH}_2\text{COOH}$ precursor molecule CH_2NH towards the G10.47+0.03 using the ACA band 4. We identified a total of three transition lines of CH_2NH towards the G10.47+0.03, and after spectral analysis using the LTE model, we observed that all identified transitions of CH_2NH are non-blended. Subsequently, these non-blended transition lines were used for rotational diagram analysis to estimate the total column density and rotational temperature of CH_2NH . Earlier, Suzuki *et al.* (2016) first attempted to search the rotational emission lines of CH_2NH from G10.47+0.03 and other hot molecular core objects. Suzuki *et al.* (2016) identified three transition lines of CH_2NH i.e., $J=4(0, 4) - 3(1, 3)$, $J=4(1, 4) - 3(1, 3)$, and $J=4(2, 3) - 3(2, 2)$ towards the G10.47+0.03 using the Nobeyama Radio Observatory (NRO) 45 m single dish telescope. Many questions arise in the detection of CH_2NH towards the G10.47+0.03 by Suzuki *et al.* (2016). First, all detected spectral lines of CH_2NH towards the G10.47+0.03 were below 2.5σ statistical significance (for details, see Fig. 3 in Suzuki *et al.* (2016)), and the authors did not use any radiative transfer model for spectral characterization of CH_2NH . Suzuki *et al.* (2016) also did not discuss the blending effect of CH_2NH with nearby molecular transitions in the molecular spectra of G10.47+0.03. The single-dish observation of CH_2NH by Suzuki *et al.* (2016) could not study the spatial distribution of CH_2NH towards G10.47+0.03. Thus, Suzuki *et al.* (2016) did not estimate any information regarding the source size or emitting region of CH_2NH , which restricted the accuracy of their measurements of the proper column density of the detected molecules. We also observed that the upper state energy (E_u) of the transition lines of CH_2NH detected by Suzuki *et al.* (2016) varies between 10 and 30 K. In the rotational diagram, lower energy levels will not enable accurate determination of the column density. In the rotational diagram, transitions at significantly higher energy levels can determine a more accurate column density. Our interferometric detection of CH_2NH using ACA gives us confidence in the more accurate column density of CH_2NH because the upper state energies of the detected transitions vary between 9 K and 240 K. From the spatial distribution analysis, we estimated that the emission regions of CH_2NH vary between $10.520'' - 10.781''$. The estimated molecular column density of CH_2NH towards the G10.47+0.03 using the ACA was $(3.40 \pm 0.2) \times 10^{15} \text{ cm}^{-2}$ with a rotational temperature of $218.70 \pm 20 \text{ K}$. Earlier, Suzuki *et al.* (2016) estimated that the column density of CH_2NH towards the G10.47+0.03 using the NRO telescope is $(4.70 \pm 1.6) \times 10^{15} \text{ cm}^{-2}$ with a rotational temperature of $84 \pm 57 \text{ K}$. We find that our estimated column density of CH_2NH is similar to that reported by Suzuki *et al.* (2016), but the temperature is different. The estimated rotational temperature of CH_2NH by Suzuki *et al.* (2016) indicates that the detected transition lines of CH_2NH arise from the cold region of G10.47+0.03. Our estimated temperature indicates that the emission lines of CH_2NH arise from the warm-inner region of G10.47+0.03. Suzuki *et al.* (2016) found the lower rotational temperature due to the lower spatial and spectral resolution of the NRO telescope. Our estimated higher excitation temperature of CH_2NH using ACA is accurate because the temperature of the hot

molecular cores is above 100 K (van Dishoeck and Blake, 1998). The other two precursors of $\text{NH}_2\text{CH}_2\text{COOH}$, such as CH_3NH_2 (Ohishi *et al.*, 2019) and $\text{NH}_2\text{CH}_2\text{CN}$ (Manna and Pal, 2022a) were also detected towards G10.47+0.03 using the NRO and ALMA telescopes. The detection of CH_2NH towards G10.47+0.03 indicates that three possible precursors of $\text{NH}_2\text{CH}_2\text{COOH}$ are present in G10.47+0.03. That means the hot molecular core G10.47+0.03 is an ideal candidate for searching the emission lines of $\text{NH}_2\text{CH}_2\text{COOH}$.

Comparison with modelled and observed abundance of CH_2NH

After estimating the fractional abundance of CH_2NH towards the G10.47+0.03, we compared the estimated abundance of CH_2NH with the modelled abundance of CH_2NH , which was estimated from the two-phase warm-up chemical model (Suzuki *et al.*, 2016). For chemical modelling, Suzuki *et al.* (2016) used the gas-grain chemical kinetics code NAUTILUS in an environment with hot molecular cores. In chemical modelling, Suzuki *et al.* (2016) assumed an isothermal collapse phase after a static warm-up phase. In the first phase, the gas density rapidly increased from 3×10^3 to $1 \times 10^7 \text{ cm}^{-3}$, and under free-fall collapse, the dust temperature decreased from 16 to 8 K. In the second phase, the gas density remained constant at $1 \times 10^7 \text{ cm}^{-3}$ and the gas temperature fluctuated rapidly from 8 to 400 K (Suzuki *et al.*, 2016). In chemical modelling, Suzuki *et al.* (2016) used the neutral–neutral reaction between CH_3 and NH radicals in the gas phase and the neutral–neutral reaction between CH_2 and NH radicals on the grain surface to create CH_2NH under the condition of hot molecular cores. The gas temperature of G10.47+0.03 was ~ 150 K (Rolffs *et al.*, 2011) and the gas density was $7 \times 10^7 \text{ cm}^{-3}$ (Rolffs *et al.*, 2011). Therefore, the two-phase warm-up chemical model of Suzuki *et al.* (2016), which is based on the time scale, is appropriate for explaining the chemical abundance and evolution of CH_2NH towards the G10.47+0.03. After the simulation, Suzuki *et al.* (2016) observed that the modelled abundance of CH_2NH varied between $\sim 10^{-9}$ – 10^{-8} in the gas phase. Similarly, the abundance of CH_2NH on the grain surface is $\leq 10^{-12}$. We found that the abundance of CH_2NH towards the G10.47+0.03 is 2.61×10^{-8} , which is nearly similar to the modelled abundance of CH_2NH in the gas phase derived by Suzuki *et al.* (2016). This result indicates that CH_2NH is created towards G10.47+0.03, via the gas-phase neutral–neutral reaction between CH_3 and NH radicals.

Previously, Manna and Pal (2022a) claimed that $\text{NH}_2\text{CH}_2\text{CN}$ was the daughter molecule of CH_2NH (see Fig. 1). The identification of both CH_2NH and $\text{NH}_2\text{CH}_2\text{CN}$ indicates that G10.47+0.03 is an ideal candidate in the ISM, where $\text{NH}_2\text{CH}_2\text{COOH}$ may exist. In ISM, G10.47+0.03 is the only source where the maximum number of possible $\text{NH}_2\text{CH}_2\text{COOH}$ precursors (such as NH_2CN , H_2CO , CH_3NH_2 , CH_2NH and $\text{NH}_2\text{CH}_2\text{CN}$) is detected, and several prebiotic chemistries have been proposed to understand the possible formation mechanism of these molecules and their possible connection with $\text{NH}_2\text{CH}_2\text{COOH}$. After detecting the maximum number of $\text{NH}_2\text{CH}_2\text{COOH}$ precursors towards the G10.47+0.03, we created a possible chemical network to understand the prebiotic chemistry of $\text{NH}_2\text{CH}_2\text{COOH}$ towards the G10.47+0.03. The chemical network is shown in Fig. 6. In the chemical network, all reactions were obtained from Woon (2002); Theule *et al.* (2011); Danger (2011); Garrod (2013); Alonso *et al.* (2018); Ohishi *et al.* (2019); Manna and Pal (2022a) and UMIST 2012 astrochemistry molecular reaction databases. The chemical network clearly indicates the maximum number of parent molecules detected towards the G10.47+0.03, which gives us an idea about the chemical complexity towards hot molecular cores.

Searching of $\text{NH}_2\text{CH}_2\text{COOH}$ towards the G10.47+0.03 using the ACA

After the identification of three possible $\text{NH}_2\text{CH}_2\text{COOH}$ precursor molecules like CH_2NH (present paper), CH_3NH_2 (Ohishi *et al.*, 2019) and $\text{NH}_2\text{CH}_2\text{CN}$ (Manna and Pal, 2022a) towards the G10.47+0.03, we searched the emission lines of $\text{NH}_2\text{CH}_2\text{COOH}$ conformers I and II towards the G10.47+0.03. After the careful spectral analysis using the LTE model, we did not detect any evidence of $\text{NH}_2\text{CH}_2\text{COOH}$ conformers I and II towards the G10.47+0.03 within the limits of our LTE

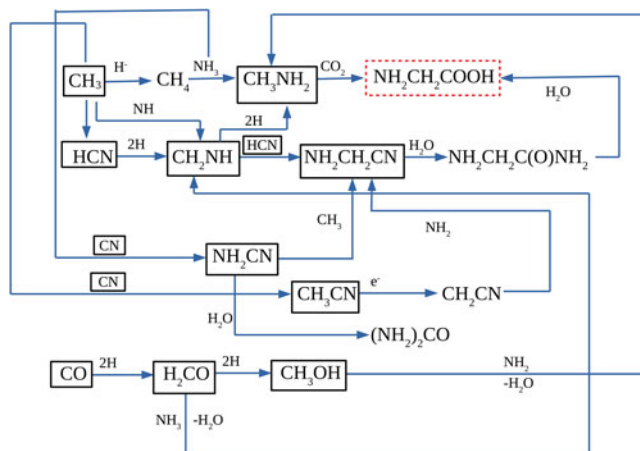


Figure 6. Proposed chemical network for the formation of $\text{NH}_2\text{CH}_2\text{COOH}$ from other molecules. In the network, the red box molecule is the final daughter molecule ($\text{NH}_2\text{CH}_2\text{COOH}$) and the black box molecules are the parent molecules that are detected towards the G10.47+0.03.

modelling. The estimated upper limit column density of $\text{NH}_2\text{CH}_2\text{COOH}$ conformers I and II towards the G10.47+0.03 was $\leq 1.02 \times 10^{15} \text{ cm}^{-2}$ and $\leq 2.36 \times 10^{13} \text{ cm}^{-2}$ respectively. The energy of $\text{NH}_2\text{CH}_2\text{COOH}$ conformer I is 705 cm^{-1} (1012 K) lower than that of $\text{NH}_2\text{CH}_2\text{COOH}$ conformer II (Lovas *et al.*, 1995). The dipole moments of $\text{NH}_2\text{CH}_2\text{COOH}$ conformer I are $\mu_a = 0.911 \text{ D}$ (a-type) and $\mu_b = 0.607 \text{ D}$ (b-type), whereas $\text{NH}_2\text{CH}_2\text{COOH}$ conformer II has dipole moments of $\mu_a = 5.372 \text{ D}$ (a-type) and $\mu_b = 0.93 \text{ D}$ (b-type) (Lovas *et al.*, 1995). In ISM, the detection of a-type³ transitions of $\text{NH}_2\text{CH}_2\text{COOH}$ are expected compared to b-type transitions because the line intensity of the molecule is proportional to the square of the dipole moments (Lovas *et al.*, 1995). The detection of three possible $\text{NH}_2\text{CH}_2\text{COOH}$ precursor molecules towards the G10.47+0.03 gives more confidence about the presence of $\text{NH}_2\text{CH}_2\text{COOH}$ towards the G10.47+0.03.

Conclusion

In this article, we present the identification of the possible $\text{NH}_2\text{CH}_2\text{COOH}$ precursor molecule CH_2NH towards the G10.47+0.03, using the ACA band 4. The main conclusions of this study are as follows:

1. We successfully identified three non-blended transition lines of CH_2NH towards the G10.47+0.03 using the ACA observation.
2. The estimated column density of CH_2NH towards the G10.47+0.03 is $(3.40 \pm 0.2) \times 10^{15} \text{ cm}^{-2}$ with a rotational temperature of $218.70 \pm 20 \text{ K}$. The estimated fractional abundance of CH_2NH towards the G10.47+0.03 with respect to H_2 is 2.61×10^{-8} .
3. We compare the estimated abundance of CH_2NH with the two-phase warm-up chemical model abundance of CH_2NH proposed by Suzuki *et al.* (2016). We noticed that the modelled abundance of CH_2NH is nearly similar to the observed abundance of CH_2NH towards the G10.47+0.03. This comparison indicates that CH_2NH is created via a gas-phase neutral–neutral reaction between CH_3 and NH radicals towards the G10.47+0.03.
4. After the successful detection of CH_2NH towards the G10.47+0.03, we also search the emission lines of the simplest amino acid $\text{NH}_2\text{CH}_2\text{COOH}$ conformers I and II towards the G10.47+0.03. We do not detect the emission lines of $\text{NH}_2\text{CH}_2\text{COOH}$ conformers I and II within the limits of

³The a-type and b-type are the different transitions of $\text{NH}_2\text{CH}_2\text{COOH}$, whose spectral parameters depend on the different electric dipole moments.

LTE modelling. The estimated upper-limit column densities of $\text{NH}_2\text{CH}_2\text{COOH}$ conformers I and II are $\leq 1.02 \times 10^{15} \text{ cm}^{-2}$ and $\leq 2.36 \times 10^{13} \text{ cm}^{-2}$ respectively.

5. The unsuccessful detection of $\text{NH}_2\text{CH}_2\text{COOH}$ towards G10.47+0.03 using ACA indicate that the emission lines of $\text{NH}_2\text{CH}_2\text{COOH}$ may be below the confusion limit in G10.47+0.03.

Acknowledgements. We thank the anonymous referees for their helpful comments, which improved the manuscript. A. M. acknowledges the Swami Vivekananda merit cum means scholarship (SVMCM), Government of West Bengal, India, for financial support for this research. The plots within this paper and other findings of this study are available from the corresponding author upon reasonable request. This paper makes use of the following ALMA data: ADS /JAO.ALMA#2016.2.00005.S. ALMA is a partnership of ESO (representing its member states), NSF (USA) and NINS (Japan), together with NRC (Canada), MOST and ASIAA (Taiwan), and KASI (Republic of Korea), in co-operation with the Republic of Chile. The Joint ALMA Observatory is operated by ESO, AUI/NRAO and NAOJ.

Competing interest. None.

References

- Allen V, van der Tak FFS, Sánchez-Monge Á, Cesaroni R and Beltrán MT (2017) Chemical segregation in hot cores with disk candidates: an investigation with ALMA. *Astronomy & Astrophysics* **603**, A133–A185.
- Alonso ER, Kolesníková L, Białkowska-Jaworska E, Kisiel Z, León I, Guillemin JC and Alonso JL (2018) Glycinamide, a glycine precursor, caught in the gas phase: a laser-ablation jet-cooled rotational study. *Astrophysical Journal* **861**, 70–77.
- Belloche A, Müller HSP, Menten KM, Schilke P and Comito C (2013) Complex organic molecules in the interstellar medium: IRAM 30 m line survey of Sagittarius B2(N) and (M). *Astronomy & Astrophysics* **559**, A47–A234.
- Bøgelund EG, McGuire BA, Hogerheijde MR, van Dishoeck EF and Ligterink NFW (2019) Methylamine and other simple N-bearing species in the hot cores NGC 6334I MM1-3. *Astronomy & Astrophysics* **624**, A82–A101.
- Cesaroni R, Hofner P, Araya E and Kurtz S (2010) The structure of hot molecular cores over 1000 AU. *Astronomy & Astrophysics* **509**, A50–A65.
- Danger G, Borget F, Chomat M, Duvernay F, Theulé P, Guillemin JC, Le Sergeant D’Hendecourt L and Chiavassa T (2011) Experimental investigation of aminoacetonitrile formation through the Strecker synthesis in astrophysical-like conditions: reactivity of methanimine (CH_2NH), ammonia (NH_3), and hydrogen cyanide (HCN). *Astronomy & Astrophysics* **535**, A47.
- Dickens JE, Irvine WM, Devries CH and Ohishi M (1997) Hydrogenation of interstellar molecules: a survey for methylenimine (CH_2NH). *Astrophysical Journal* **479**, 307–312.
- Garrod RT (2013) A three-phase chemical model of hot cores: the formation of glycine. *Astrophysical Journal* **765**, 60–89.
- Garrod RT and Herbst E (2006) Formation of methyl formate and other organic species in the warm-up phase of hot molecular cores. *Astronomy & Astrophysics* **457**, 927–936.
- Garrod RT, Jin M, Matis KA, Jones D, Willis ER and Herbst E (2022) Formation of complex organic molecules in hot molecular cores through nondiffusive grain-surface and ice-mantle chemistry. *Astrophysical Journal Supplement* **259**, 1–71.
- Godfrey PD, Brown RD, Robinson BJ and Sinclair MW (1973) Discovery of interstellar methanimine (formaldimine). *Astrophysical Letters* **13**, 119–121.
- Goldsmith PF and Langer WD (1999) Population diagram analysis of molecular line emission. *Astrophysical Journal* **517**, 209–225.
- Gorski MD, Aalto S, Mangum J, Momjian E, Black JH, Falstad N, Gullberg B, KÖnig S, Onishi K, Sato M and Stanley F (2021) Discovery of methanimine (CH_2NH) megamasers toward compact obscured galaxy nuclei. *Astronomy & Astrophysics* **654**, A110–A123.
- Halfen DT, Ilyushin VV and Ziurys LM (2013) Insights into surface hydrogenation in the interstellar medium: observations of methanimine and methyl amine in Sgr B2(N). *Astrophysical Journal* **767**, 66–77.
- Herbst E and van Dishoeck EF (2009) Complex organic interstellar molecules. *Annual Review of Astronomy and Astrophysics* **47**, 427–480.
- Jones PA, Burton MG, Cunningham MR, Menten KM, Schilke P and Belloche A (2008) Spectral imaging of the Sagittarius B2 region in multiple 3-mm molecular lines with the Mopra telescope. *Monthly Notices of the Royal Astronomical Society* **386**, 117–137.
- Jones PA, Burton MG, Tothill NFW and Cunningham MR (2011) Spectral imaging of the Sagittarius B2 region in multiple 7-mm molecular lines. *Monthly Notices of the Royal Astronomical Society* **411**, 2293–2310.
- Joshi PR and Lee YP (2022) A chemical link between methylamine and methylene imine and implications for interstellar glycine formation. *Communications Chemistry* **5**, 62–69.
- Kirchhoff WH, Johnson DR and Lovas FJ (1973) Microwave spectra of molecules of astrophysical interest: ii methylenimine. *Journal of Physical and Chemical Reference Data* **2**, 1.
- Kurtz S, Cesaroni R, Churchwell E, Hofner P and Walmsley CM (2000) Hot molecular cores and the earliest phases of high-mass star formation. *Protostars and Planets* **IV**, 299–326.

- Ligterink NFW, Calcutt H, Coutens A, Kristensen LE, Bourke TL, Drozdovskaya MN, Müller HSP, Wampfler SF, van der Wiel MHD, van Dishoeck EF and Jørgensen JK (2018) The ALMA-PILS survey: stringent limits on small amines and nitrogen-oxides towards IRAS 16293-2422B. *Astronomy & Astrophysics* **619**, A28–A39.
- Lovas FJ, Kawashima Y, Grabow JU, Suenram RD, Fraser GT and Hirota E (1995) Microwave spectra, hyperfine structure, and electric dipole moments for conformers i and ii of glycine. *Astrophysical Journal* **455**, L201–L204.
- Manna A and Pal S (2022a) Identification of interstellar amino acetonitrile in the hot molecular core G10.47+0.03: possible glycine survey candidate for the future. *Life Sciences in Space Research* **34**, 9–15.
- Manna A and Pal S (2022b) Detection of interstellar cyanamide (NH₂CN) towards the hot molecular core G10.47+0.03. *Journal of Astrophysics and Astronomy* **43**, 83–93.
- Manna A and Pal S (2022c) First detection of methyl formate in the hot molecular core IRAS 18566+0408. *Astrophysics and Space Science* **367**, 94–104.
- Manna A and Pal S (2023a) Detection of complex nitrogen-bearing molecule ethyl cyanide towards the hot molecular core G10.47+0.03. *Astrophysics and Space Science* **368**, 44–56.
- Manna A and Pal S (2023b) Detection of monothioformic acid towards the solar-type protostar IRAS 16293–2422. *Journal of Astrophysics and Astronomy* **44**, 69–78.
- Manna A and Pal S (2024a) Detection of possible glycine precursor molecule methylamine towards the hot molecular core G358.93–0.03 MM1. *New Astronomy* **109**, 102199–102208.
- Manna A and Pal S (2024b) ACA observation and chemical modeling of phosphorus nitride towards hot molecular cores G10.47+0.03 and G31.41+0.31. *Journal of Astrophysics and Astronomy* **45**, 3–12.
- Manna A and Pal S (2024) Detection and chemical modeling of complex prebiotic molecule cyanamide in the hot molecular core G31.41+0.31. *ACS Earth and Space Chemistry* **4**, 665–674.
- Manna A, Pal S, Viti S and Sinha S (2023) Identification of the simplest sugar-like molecule glycolaldehyde towards the hot molecular core G358.93–0.03 MM1. *Monthly Notices of the Royal Astronomical Society* **525**, 2229–2240.
- McMullin JP, Waters B, Schiebel D, Young W and Golap K (2007) CASA architecture and applications, Astronomical Society of the Pacific Conference Series, Vol. 376, Astronomical Data Analysis Software and Systems XVI, Shaw R. A., Hill F. and Bell D. J., p. 127–130.
- Müller HSP, Schlmöder F, Stutzki J and Winnewisser G (2005) The cologne database for molecular spectroscopy, CDMS: a useful tool for astronomers and spectroscopists. *Journal of Molecular Structure* **742**, 215–227.
- Ohishi M, Suzuki T, Hirota T, Saito M and Kaifu N (2019) Detection of a new methylamine (CH₃NH₂) source: candidate for future glycine surveys. *Publications of the Astronomical Society of Japan* **71**, 86–97.
- Perley RA and Butler BJ (2017) An accurate flux density scale from 50 MHz to 50 GHz. *Astrophysical Journal Supplement* **204**, 19–37.
- Qin S-L, Wu Y, Huang M, Zhao G, Li D, Wang J-J and Chen S (2010) High-resolution submillimeter multiline observations of G19.61-0.23: small-scale chemistry. *Astrophysical Journal* **711**, 399–416.
- Rivilla VM, Beltrán MT, Cesaroni R, Fontani F, Codella C and Zhang Q (2017) Formation of ethylene glycol and other complex organic molecules in star-forming regions. *Astronomy & Astrophysics* **598**, A59–A82.
- Rolffs R, Schilke P, Zhang Q and Zapata L (2011) Structure of the hot molecular core G10.47+0.03. *Astronomy & Astrophysics* **536**, A33–A56.
- Sanna A, Reid MJ, Menten KM, Dame TM, Zhang B, Sato M, Brunthaler, A, Moscadelli L and Immer K (2014) Trigonometric parallaxes to star-forming regions within 4 kpc of the galactic center. *Astrophysical Journal* **781**, 108–121.
- Shimonishi T, Izumi N, Furuya K and Yasui C (2021) The detection of a hot molecular core in the extreme outer galaxy. *Astrophysical Journal* **2**, 206–245.
- Sutton EC, Jaminet PA, Danchi WC and Blake GA (1991) Molecular line survey of sagittarius B2(M) from 330 to 355 GHz and comparison with sagittarius B2(N). *Astrophysical Journal Supplement* **77**, 255–285.
- Suzuki T, Ohishi M, Hirota T, Saito M, Majumdar L and Wakelam V (2016) Survey observations of a possible glycine precursor Methanimine (CH₂NH). *Astrophysical Journal* **825**, 79–94.
- Tan JC, Beltrán MT, Caselli P, Fontani F, Fuente A, Krumholz MR, McKee CF and Stolte A (2014) Massive star formation. *Protostars and Planets VI*, 149–172.
- Theule P, Borget F, Mispelaer F, Danger G, Duvernay F, Guillemin JC and Chiavassa T (2011) Hydrogenation of solid hydrogen cyanide HCN and methanimine CH₂NH at low temperature. *Astronomy & Astrophysics* **534**, A64–A70.
- Turner BE (1989) A molecular line survey of sagittarius B2 and Orion-KL from 70 to 115 GHz. I. The observational data. *Astrophysical Journal Supplement* **70**, 539–622.
- van Dishoeck EF and Blake GA (1998) Chemical evolution of star-forming regions. *Annual Review of Astronomy and Astrophysics* **36**, 317–368.
- Vastel C, Bottinelli S, Caux E, Glorian J-M and Boiziot M (2015) Cassis: a tool to visualize and analyse instrumental and synthetic spectra, Proceedings of the Annual meeting of the French Society of Astronomy and Astrophysics, pp. 313–316.
- White GJ, Araki M, Greaves JS, Ohishi M and Higginbottom NS (2003) A spectral survey of the Orion Nebula from 455–507 GHz. *Astronomy & Astrophysics* **407**, 589–607.
- Woon DE (2002) Pathways to glycine and other amino acids in ultraviolet-irradiated astrophysical ices determined via quantum chemical modeling. *Astrophysical Journal* **571**, L177–L180.